Two-dimensional resonances in Alpine valleys identified from ambient vibration wavefields

D. Roten, D. Fäh, C. Cornou* and D. Giardini

Institute of Geophysics, ETH Hönggerberg, 8093 Zürich, Switzerland. E-mail: daniel.roten@sed.ethz.ch

SUMMARY

Although numerical simulations have for long shown the importance of 2-D resonances in site effect estimations of sediment-filled valleys, this phenomenon is usually not taken into account by current hazard assessment techniques. We present an approach to identify the resonance behaviour of a typical Alpine valley by analysis of ambient noise recorded simultaneously on a dense array. The applicability of the method is evaluated further using synthetic ambient noise acquired with current 3-D numerical simulation techniques. Resonance frequencies of the fundamental mode *SV* and the fundamental and first higher mode of *SH* are identified from measured data with the reference station method, verifying results of previous studies. Patterns of spectral amplitude and phase behaviour obtained from observed and synthetic noise correlate well with properties expected for 2-D resonance. Application of a frequency-wavenumber technique shows that the noise wavefield is dominated by standing waves at low frequencies (0.25 to 0.50 Hz). The different 2-D resonance modes are creating prominent peaks in horizontal-to-vertical spectral ratios, which can not be interpreted in terms of 1-D resonance. We conclude that ambient noise records measured simultaneously on a linear array perpendicular to the valley axis may be used for identification of resonance modes in sediment-filled valleys.

Key words: Rhône valley, sedimentary basin, seismic array, seismic noise, spectral analysis, synthetic waveforms.

GJI Seismology

1 INTRODUCTION

It is well established that site-effects caused by unconsolidated deposits must be included in hazard assessments, and instrumental and numerical techniques are now widely used to estimate amplifications caused by 1-D site effects. However, numerical simulations have for long demonstrated the importance of considering 2-D or 3-D geometries, since effects related to such structures can cause amplifications significantly higher than the corresponding 1-D values (e.g. Bard & Bouchon 1985).

Sediment-filled Alpine valleys are common examples of such 2-D-sites. Depending on the valley geometry, two different effects can be distinguished:

(i) In rather shallow valleys, the wavefield is dominated by laterally propagating surface waves generated at the valley edges. This effect is often observed in both synthetic (e.g. Bard & Bouchon 1980) and measured data (e.g. Field 1996; Chávez-García *et al.* 2003). Lateral variations of the interface between bedrock and sediments can give rise to local 1-D resonances (Fäh *et al.* 1993).

*Now at: LGIT, Maison des Geosciences, BP53, 38041 Grenoble Cedex9, France.

(ii) In deeper valleys, the interference of these surface waves with vertically propagating waves gives rise to the evolution of a 2-D resonance pattern. Although this phenomenon evolved in many numerical simulations (e.g. Bard & Bouchon 1985; Frischknecht & Wagner 2004), observations on real data are rare (e.g. Kagami *et al.* 1982; Tucker & King 1984; King & Tucker 1984).

Most attempts to identify and quantify these effects involved measurements of earthquake motion on different sites on the sediment fill and on the outcropping rock, using array-based (e.g. Cornou *et al.* 2003) or reference station dependent (e.g. Chávez-García *et al.* 2003) methods. In regions with low seismicity, site effect estimations with these procedures would require long and thereby expensive measurement campaigns. Methods based on quick and cheaper microtremor measurements for identification and quantification of such 2-D-effects would, therefore, be desirable.

Numerical microtremor simulations performed by Steimen *et al.* (2003) showed that 2-D resonance in a sediment filled valley can be excited by laterally-incident microtremor waves. Steimen *et al.* (2003) applied a site-to-reference technique to synthetic microtremor records obtained with a realistic model of the Rhône valley near Vétroz (Switzerland), demonstrating the capability of the method to identify the resonance frequencies of the site. The

method was also applied to observed microtremor recordings measured simultaneously at the reference site and at one location on the sediment fill for different points across the valley. However, this approach did not allow a comparison of amplification and phase characteristics of records acquired at different positions, since the wavefield was not measured simultaneously at all points. The peaks in spectral ratios obtained from observed microtremors could, therefore, not unambiguously be identified as 2-D resonance modes.

In order to verify the results obtained from the numerical simulations of Steimen *et al.* (2003), we present results of two new measurement campaigns involving simultaneous recording of the noise wavefield on 13 sites on the sediment fill and on the outcropping rock at the Vétroz site.

To take advantage of recent developments in the field of ambient noise research, we repeated the numerical simulation of Steimen *et al.* (2003) for the same geophysical model, but a 3-D computational region and a different noise source definition, using a code developed within the European SESAME (site effects assessment using ambient excitations) project (Moczo & Kristek 2002).

We will apply the site-to-reference technique to these synthetic and recorded data to seek for characteristic patterns of 2-D resonance in the microtremor wavefield. Additionally, we will introduce a method to analyse the phase behaviour of microtremor records at the resonance frequencies. We will put special emphasis on the problem of distinguishing between laterally propagating surface waves and 2-D-resonance, since this issue gave rise to some discussion in recent publications (Paolucci & Faccioli 2003; Chávez-García & Stephenson 2003).

Using results of this synthetic and recorded microtremor analysis, we will try to evaluate the suitability of microtremor records for 2-D site effect assessment.

2 GEOPHYSICAL SETTING

The Rhône valley is a deeply eroded basin filled with glacial and post-glacial Quaternary sediments. In the framework of a national research project, the sedimentary fill and shape of the valley was investigated using high-resolution reflection seismic lines, with one profile running perpendicular to the valley axis at the Vétroz site (Pfiffner *et al.* 1997). Based on results of this cross-section, Steimen *et al.* (2003) created a realistic geophysical model of the Vétroz site, only simplified by the introduction of horizontal layers (Fig. 1). Interface depths and *P*-wave velocities (Table 1) are provided directly by seismic reflection data (Pfiffner *et al.* 1997). Shear wave velocities at the uppermost layer are derived from a shallow shear–wave refraction experiment done near Vétroz (Frischknecht 2000); Steimen *et al.* (2003) estimated shear–wave velocities for lower layers. The quality factors Q_p and Q_s are estimated as well, and densities are
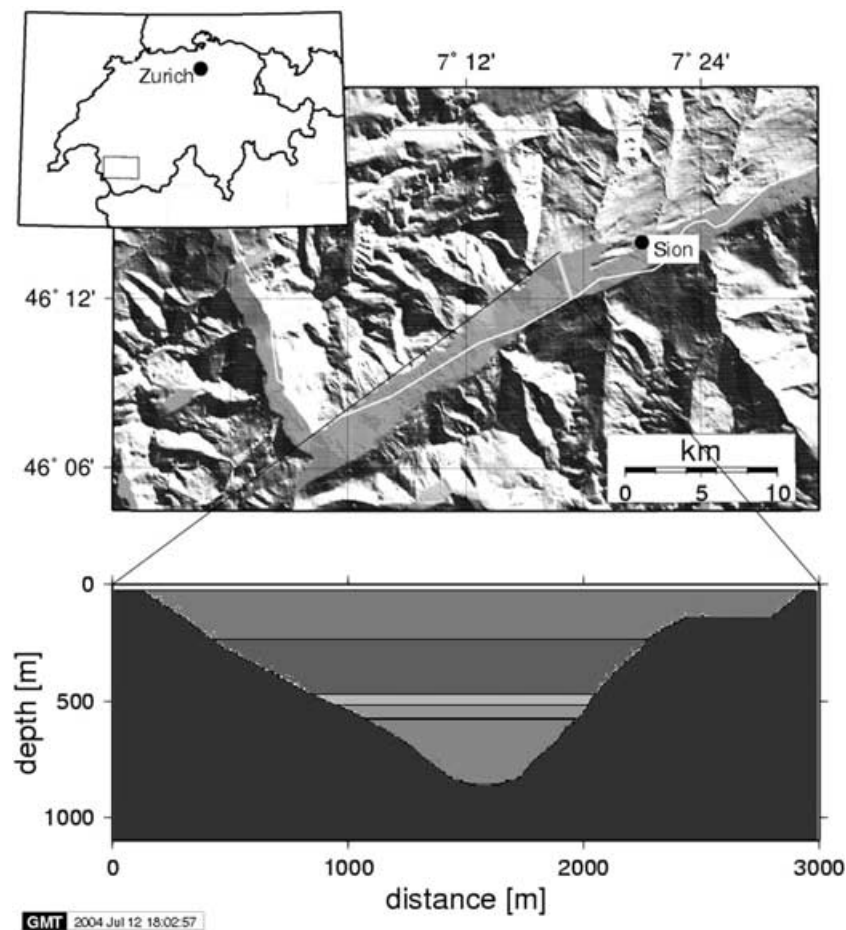
Figure 1. Cross-section of Rhône valley at Vétroz site. See Table 1 for details of sediment fill. (modified from Steimen *et al.* 2003). Reproduced by permission of swisstopo (BA057507).

Table 1. Geophysical model of the sediment fill. Depths are in m, v_p and v_s in ms^{-1} and ρ in kgm^{-3}.

depth	v_p	v_s	Q_p	Q_s	ρ	Geologic interpretation
0	1700	456	50	25	1900	Deltaic sediments
210	1930	650	50	25	1900	Glaciolacustrine deposits
470	1970	790	50	25	2000	Meltout and reworked till
529	2300	920	50	25	2000	Lodgment and till
584	2050	820	50	25	2000	Subglacial deposit
890	5000	2890	200	100	2500	Hard rock

available through gravimetric studies (summarized in Frischknecht 2000). To obtain a mean value $\bar{v}$ for the velocities of the whole sediment fill, we use the traveltime-based average:

$$\frac{1}{\bar{v}} = \frac{1}{H} \sum_{i=1}^{n} \frac{h_i}{v_i} \quad \text{with} \quad H = \sum_{i=1}^{n} h_i, \tag{1}$$

where h_i is the the thickness of layer i. For the velocities in Table 1, this yields $\bar{v}_p = 1929$ ms^{-1} and $\bar{v}_s = 651$ ms^{-1}.

3 THEORY

3.1 1-D and 2-D resonance

1-D resonance is caused by the trapping of body waves in soft horizontally layered sediments overlying solid bedrock. The 1-D resonance frequency f_h depends on the layer thickness h and the shear-wave velocity v_s of the sedimentary layer:

$$f_h = \frac{v_s}{4h}. \tag{2}$$

If local 1-D resonance develops in shallow basins, the resonance frequency will depend on the position in the valley and reflect the local sediment thickness.

In the case of 2-D resonance, however, the resonance frequency is the same across the whole valley (Bard & Bouchon 1985; King & Tucker 1984; Tucker & King 1984; Kagami *et al.* 1982). The frequencies of 2-D resonance modes are higher than the 1-D resonance frequency f_h at the valley centre. As Bard & Bouchon (1985) demonstrated, the frequency of mode SH_{00} is slightly above f_h for shallow valleys and increases with increasing valley depth. The frequencies observed in the case of 2-D resonance can, therefore, not be explained with 1-D analysis of the sediment fill.

Since the shear-wave velocity of the sediments are well known for our site, we will reveal the importance of 2-D resonance effects by comparison of identified peak frequencies with theoretical 1-D values. With the traveltime-based shear-wave velocity average calculated above, an approximate 1-D resonance frequency of 0.18 Hz can be derived for the valley centre from eq. (2).

For large velocity contrasts the ellipticity of the fundamental mode Rayleigh wave has infinite values close the fundamental frequency of resonance (e.g. Asten 2004). This is shown from 1-D analysis of Rayleigh wave dispersion and ellipticity (Fig. 2) using the stratigraphy from Table 1. The 1-D resonance frequency is reflected by the peak in the fundamental mode ellipticity curve at 0.21 Hz, which is not too different from the value obtained with the traveltime-based shear-wave velocity average.
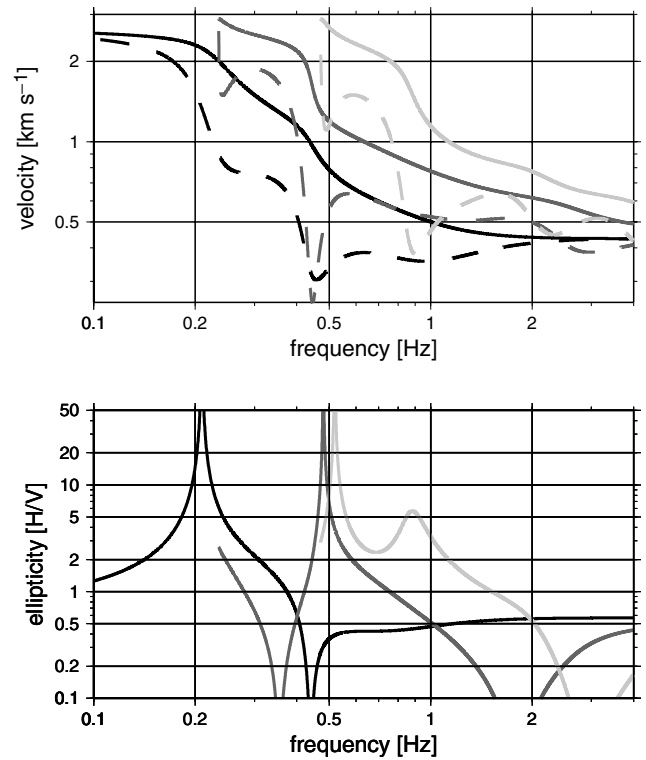
Figure 2. 1-D dispersion analysis of velocity model given in Table 1 *Top:* Phase (solid) and group velocities (dashed) for fundamental (black), first (dark grey) and second (light grey) higher mode Rayleigh waves. *Bottom:* Particle-motion horizontal/vertical ratios for the same modes, same model. (These values were computed using software from Hermann 2002).

3.2 Properties of 2-D resonance modes

3.2.1 Three fundamental modes

Using the technique from Aki & Larner (1970) to simulate the seismic behaviour of a sine shaped valley on incident *SH*, *SV* and *P*-waves, Bard & Bouchon (1985) showed the existence of three fundamental modes. We will follow the nomenclature of Field (1996) in this paper and use the terms perpendicular and axial for horizontal motion perpendicular and parallel, respectively, to the valley axis (Fig. 3). Only the axial component is excited in the *SH*-mode, while the *SV*- and *P*-mode excite both the perpendicular
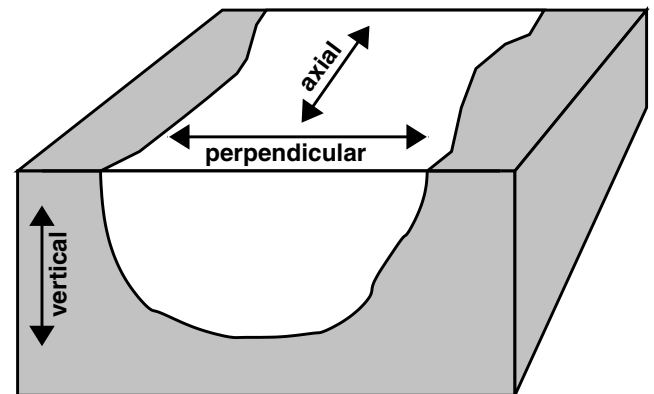
**Figure 3.** Naming convention for directions used in this text.
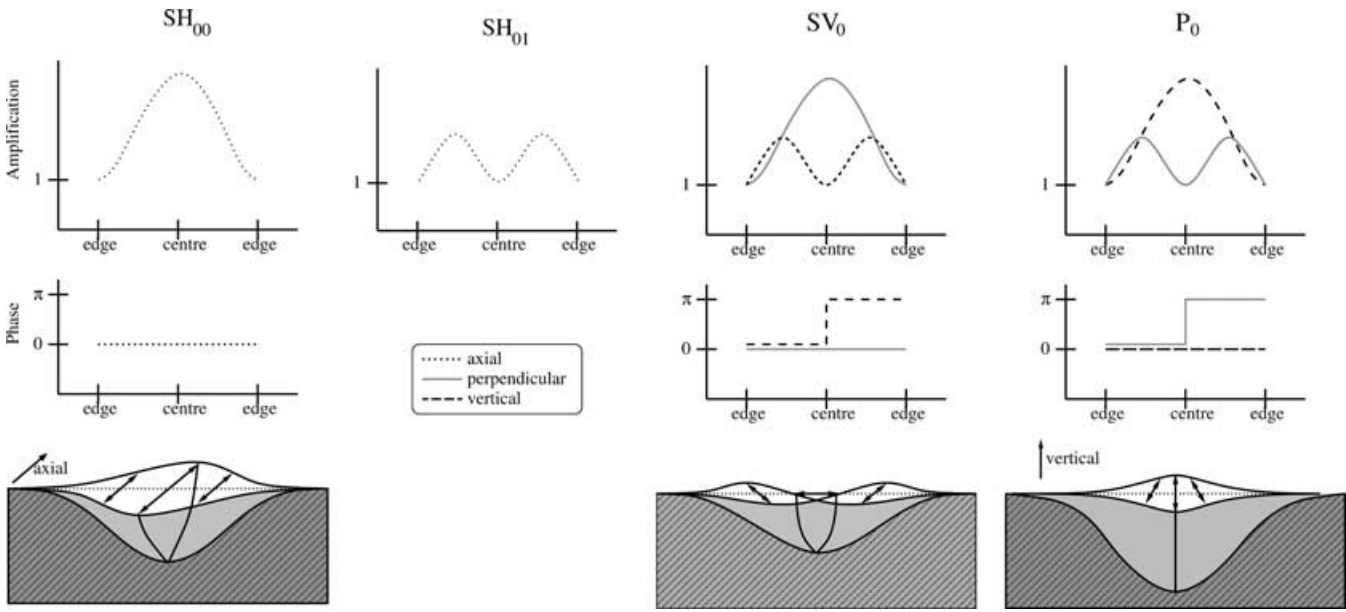
Figure 4. Amplification, phase and particle motion of the three fundamental modes of a sine shaped valley for the corresponding critical shape ratio (modified from Bard & Bouchon 1985; Steimen *et al.* 2003) and amplification for the first higher mode SH_{01}.

and vertical component (Fig. 4). In the fundamental mode SH_{00}, the phase is the same across the valley, and the amplification reaches its maximum in the valley centre. At the first higher mode SH_{01} the amplification exhibits a central node and two peaks. The SV_0 fundamental mode is characterized by a maximum amplification in the centre for the perpendicular component and a central node and two maxima for the vertical component. In this mode, the phase is the same across the valley for the perpendicular component, while the phase of the vertical motion changes at the valley centre. The P_0 fundamental mode behaves just vice-versa (Fig. 4).

3.2.2 Shape ratio

Since 2-D resonance patterns involve both vertical and horizontal interferences, they can only appear in relatively deep valleys. To identify valleys whose seismic behaviour is characterized by 2-D resonance, Bard & Bouchon (1985) introduced the concept of the *critical shape ratio*. For sine-shaped valleys, the shape ratio is defined as the ratio of the maximum sediment thickness h to the valley half-width l. For arbitrarily shaped valleys, this parameter is replaced by the 'equivalent' shape ratio $h/2w$, where $2w$ is defined as the total width over which the sediment thickness is greater than half its maximum value. The critical shape ratio depends on the velocity contrast between bedrock and sediment fill (Fig. 5). If the shape ratio of a valley is above the critical value, it's seismic behaviour at low frequencies will be characterized by 2-D resonance. The critical shape ratio depends also on the wave type; it's value is higher for *P*-waves than for *SH*- and *SV*-waves (Fig. 4).

Using 1350 m for $2w$ and 890 m for h (Pfiffner *et al.* 1997), we can assign a shape ratio of about 0.65 to the Rhône valley at the Vétroz site. The velocity contrast between bedrock and sediment fill ranges from 3.5 (subglacial deposits) to 6.4 (deltaic sediments). In Fig. 5, the shape ratio of the Vétroz site for both velocity contrasts is indicated in the diagram, showing that this site is clearly located in the domain of 2-D resonance for the *SH*-case.
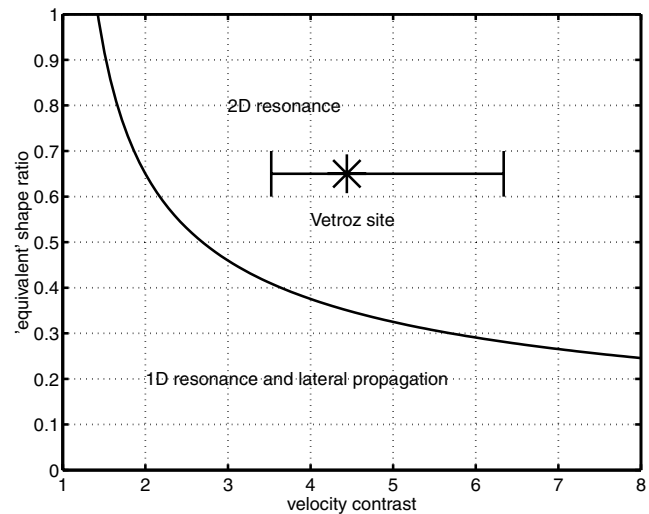

Figure 5. Critical shape ratio as a function of the velocity contrast for the *SH* case. The velocity contrasts obtained from the shear–wave velocities in Table 1 are indicated at the shape ratio of 0.65. The asterisk denotes the velocity contrast obtained with the traveltime–based shear–wave velocity average from eq. (1). (modified from Bard & Bouchon 1985).

3.2.3 Paolucci's method

Based on Rayleigh's principle, Paolucci (1999) developed a method which allows a quick calculation of the resonance frequencies of valleys filled with stratified sediments. Equating the total kinetic energy $T_{\max}$ of the system Ω with the total strain energy $V_{\max}$, the following expression can be derived, which denotes an upper bound for the true fundamental frequency ω_0:

$$\omega_0^2 \leq \min_{\hat{\psi}_k} \frac{\int_\Omega \hat{\sigma}_{jl}(\vec{x})\hat{\epsilon}_{jl}(\vec{x})\,d\Omega}{\int_\Omega \rho(\vec{x})\hat{\psi}_k^2(\vec{x})\,d\Omega}, \tag{3}$$

where $\hat{\epsilon}_{jl}$ is the strain tensor, $\hat{\sigma}_{jl}$ the stress tensor, ρ the density and $\vec{x}$ the position in 3-D space. $\hat{\psi}_k$ stands for a set of admissible
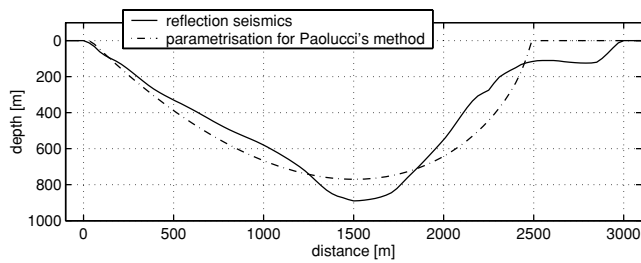
Figure 6. Sediment-bedrock interface of the Rhône valley at the Vétroz site derived from reflection seismics and described by eq. (4) with $a = 1120$ m, $h = 770$ m and $\zeta = 0.20$ (modified from Schmid 2000).

Table 2. Resonance frequencies [Hz] calculated with the method of Paolucci (1999) compared to values observed and measured by Steimen *et al.* (2003) and in this study.

	SV_0	SH_{00}	SH_{01}	SH_{02}
Paoluccis' method	0.34	0.31	0.39	0.47
Steimen modelled	0.34 ± 0.01	0.29 ± 0.02	0.38 ± 0.01	0.47 ± 0.01
Steimen observed	0.35 ± 0.03	0.32 ± 0.03		
3-D simulation	0.35 ± 0.03	0.30 ± 0.03	0.39 ± 0.04	
2002 experiment	0.35 ± 0.03	0.31 ± 0.03	0.43 ± 0.04	
2003 experiment	0.39 ± 0.03	0.35 ± 0.04	0.43 ± 0.04	

approximations of the true shape function ψ (refer to Paolucci 1999, for a detailed description).

Paolucci's program includes four functions to describe the sediment-bedrock interface. The function most appropriate for the Vétroz site denotes the shape of an asymmetric valley:

$$f(x_1, x_3) = \left(1 + \frac{x_1}{a}\right)\left(1 - \frac{x_1}{a}\right)^{\frac{1-\zeta}{1+\zeta}} - (1+\zeta)(1-\zeta)^{\frac{1-\zeta}{1+\zeta}} \cdot \frac{x_3}{h},$$
(4)

where a is the valley half-width, h the maximum depth and ζ a coefficient describing the grade of asymmetry. Fig. 6 shows the true sediment-bedrock interface of the Rhône valley at the Vétroz site and the function described by eq. (4) with $a = 1120$ m, $h = 770$ m and $\zeta = 0.20$.

Using the geophysical model given in Table 1 and four different shape functions, Schmid (2000) calculated the *SV* resonance frequencies of the Rhône valley near Vétroz and found values very similar to those reported by Steimen *et al.* (2003).

Table 2 lists the fundamental mode *SV* and the fundamental and higher modes *SH* frequencies calculated with Paolucci's method using the sediment-bedrock interface from Fig. 6. The frequencies reported by Steimen *et al.* (2003) are also given in the table. The values obtained with Paolucci's approach are equal to or slightly higher than those from the numerical simulation of Steimen *et al.* (2003), which demonstrates the capability of the method to provide an upper bound for the 2-D resonance frequencies.

As expected, the 2-D resonance frequencies are substantially higher than the theoretical 1-D resonance frequency calculated above.

3.3 Origin of noise

Studies on the nature of noise (Bonnefoy-Claudet *et al.* 2004) agree that different sources contribute to the noise wavefield at different frequency bands (Gutenberg 1958; Asten 1978; Asten & Henstridge 1984). In general, low-frequency noise (<0.5 Hz) can be assigned to coastal waves, large-scale meteorological perturbations and cy-

clones over the oceans (noise in this frequency band was referred to as *microtremor* energy by Steimen *et al.* 2003). Noise around 1 Hz can be traced to local meteorological conditions, and noise above 1 Hz to human activities (Bonnefoy-Claudet *et al.* 2004).

According to this scheme, the resonance of the structure at Vétroz should mainly be excited by far sources, since the resonance frequencies are well below 0.5 Hz. Indeed Steimen *et al.* (2003) simulated the microtremor wavefield by a source zone far away from the valley. However, the boundary between oceanic, large scale meteorological and human, small scale meteorological noise is not an universal limit, but can be shifted to lower frequencies in deep soft basins (Seo 1997).

It can, therefore, not be excluded that sources capable of exciting 2-D resonance exist within the valley. Thus we used a different source definition for our numerical simulations and placed all sources within the valley on the sediment surface, simulating man-made noise typical of densely populated urban areas.

4 METHOD

The experiments with real and simulated data were designed for a simultaneous examination of phase behaviour, amplitude and particle motion at different positions across the valley.

4.1 Field experiments

The noise wavefield at the Vétroz site was recorded during two measurement campaigns carried out in 2002 May and 2003 November.

4.1.1 2002 May experiment

The first campaign aimed to validate the results of Steimen *et al.* (2003) by simultaneous measurement of the noise wavefield at all points across the profile and at two reference stations. The positions of the stations during the 2002 experiment are denoted by rectangles in Fig. 7. Seven stations were deployed on a profile perpendicular to the axis of the valley, with shorter inter-station distances on the northern part. Four stations were set up outside the profile around the middle of the valley to form a small array; these stations are necessary to distinguish between laterally propagating surface waves and global resonance. The remaining two stations were used as reference stations on the North and on the South side of the profile on well-defined bedrock sites.

The noise wavefield was measured by 13 three-component sensors with a natural period of 5 s and recorded using DCF77 long-wave radio time signals for synchronization. The 2002 experiment resulted in about 90 min of high-quality data with very few sources of local noise in the frequency range of interest (below about 1 Hz), with the exception of the reference station in the South, which was located close to a busy road.

The evaluation of the microtremor wavefield recorded during this first experiment yielded promising results, but also raised a couple of new questions, which led us to prepare a second experiment.

4.1.2 2003 November experiment

The second campaign was designed to investigate the resonance properties with a higher spatial resolution across the profile. Therefore, all 13 stations were first put on a line running parallel to the profile of the first experiment (Circles and triangles in Fig. 7). The
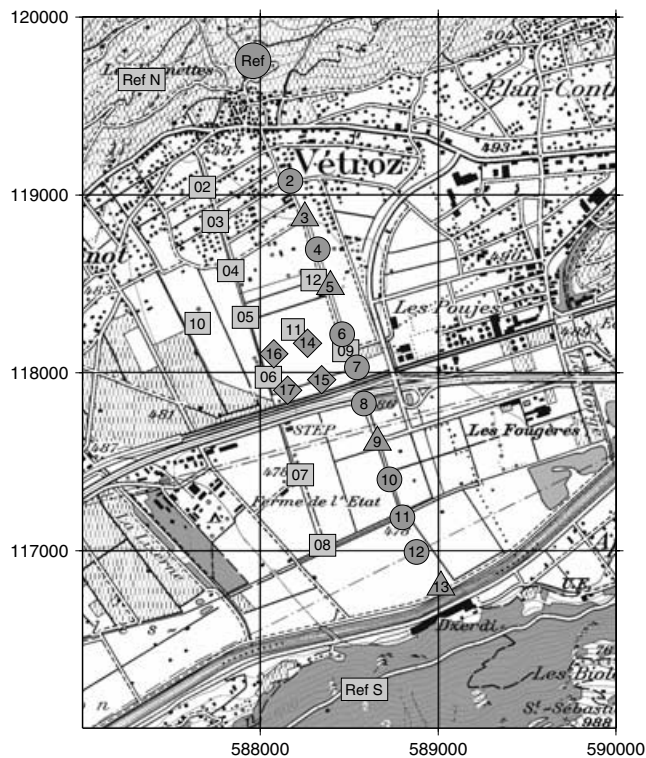
Figure 7. Configurations used for noise measurements near Vétroz. Station positions of the 2002 experiment are indicated by Light grey rectangles, those of the 2003 experiment by Dark grey circles, triangles and diamonds. Ticks denote the Swiss coordinate system in meters. Reproduced by permission of swisstopo (BA057507).

noise wavefield was measured for about 100 min with this configuration. In order to distinguish between propagation and resonance, we removed four stations (triangles) from the profile axis and placed them away from the profile in the valley centre (diamonds in Fig. 7). With this set-up, the noise wavefield was recorded during 120 more minutes.

Due to an improperly connected sensor cable, no data was recorded by station 5 for the first part of the experiment. Records acquired by station 6 contain a lot of disturbances of unknown origin, which induce low-frequency spikes in the noise traces. Fig. 8 (top) compares a low-pass filtered trace from station 6 to an undisturbed trace from station 7 and shows how such a spike influences the amplitude spectrum of the signal. These spikes at station 6 are the main reason for the introduction of the antitrigger in the spectral ratio method (see below).

Apart from stations 5 and 6, the data collected during the second measurement campaign is of satisfactory quality.

4.2 Reference station method

The reference station approach is based on the assumption that the signal at the reference site represents the signal at the sediment-bedrock interface, which implies that source and path effects at both sites must be equal. The ratio of the Fourier spectra amplitude is used to estimate the transfer function between soil and rock site (e.g. Borcherdt 1970; Lermo & Chávez-García 1994). When applied on earthquake data, the reference station method uses only the intense *S*-wave part of the seismograms. Applications on mi-
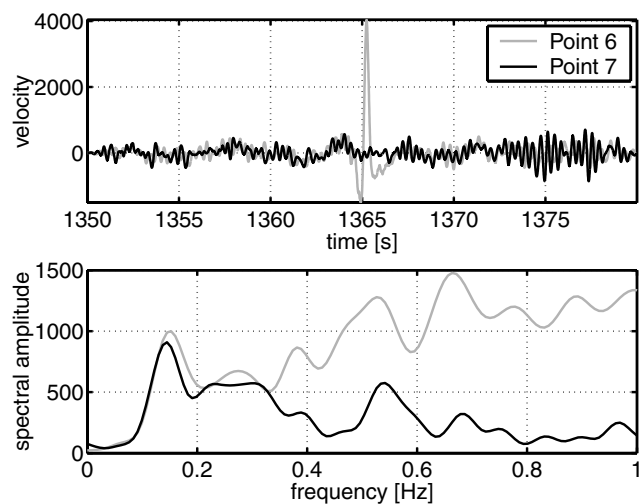
Figure 8. Comparison between disturbed (grey) and undisturbed (black) signals. Time series (top) were low-pass filtered below 1 Hz.

crotremors exploit the whole record regardless of the shape of the signals.

We used a code similar to the one applied by Steimen *et al.* (2003) for the calculation of reference spectra. Time series are split into 50 per cent overlapping windows of 80 s length and tapered with a trapezoidal window. For each time window, the ratio of the smoothed Fourier amplitudes is computed. Then the weighted average of all windows is calculated.
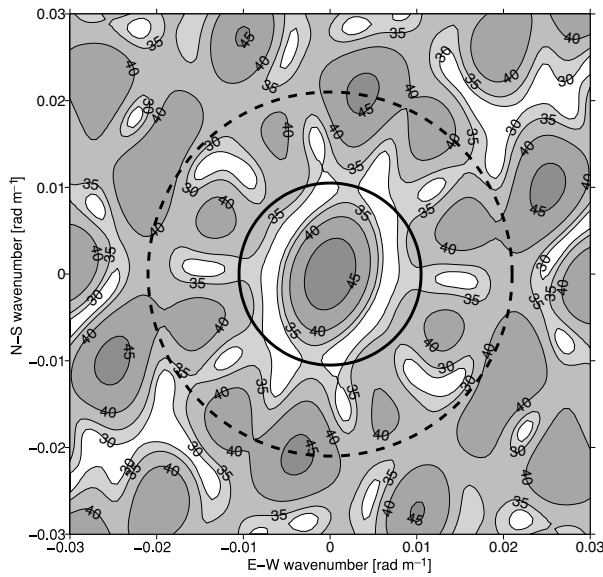
We introduced data weighting to remove effects related to low-frequency disturbances similar to the example in Fig. 8. The weighting for each window is determined by a simple suppression trigger applied to each time series after low-pass filtering with a cut-off of 1 Hz. If the amplitude of any component at any station exceeds a certain threshold value in a time window, the weighting of this window is set to zero for all stations.

4.3 Analysis of phase behaviour

The phase behaviour of motion at the fundamental mode resonance frequencies is a remarkable property of 2-D resonance (Fig. 4). The simultaneous measurement of the noise wavefield at all points allows us to analyse this effect. We expect the noise wavefield to exhibit a clear pattern of in-phase and antiphase behaviour at the fundamental mode *SV* and *SH* resonance. Time series of the axial and perpendicular component bandpass filtered around the *SH* and *SV* fundamental mode resonance frequency should be in phase at all points on the profile. For vertical traces bandpass filtered around the SV_0 frequency, the phase is expected to change around the valley centre.

The phase behaviour of short sections can easily be revealed by plotting traces next to each other. In order to analyse longer (>1 hr) time series, we will use a more systematic approach to reveal the dominant phase properties:

The phase of the motion at each point is compared to the motion at a reference point in the middle of the valley. Signals are bandpass filtered around the resonance frequency identified with spectral ratios. The cross-correlation of each filtered signal against the signal at the reference position is calculated, with a maximum lag of two seconds. The lag where the cross-correlation reaches its maximum reveals the dominant phase behaviour: if both signals are

Figure 9. Beam pattern of array used for f–k analysis of 2002 experiment. Contour intervals are indicating the array response in dB. The first aliasing peaks are located on the dashed circle and the wavenumber domain that can be analysed with this configuration is within the solid circle.

f–k spectra from the array formed by seven stations deployed during the 2002 experiment (stations 04, 05, 06, 09, 10, 11 and 12 in Fig. 7). To avoid difficulties associated with the antiphase behaviour of the vertical component in the SV_0-case, all stations used for the f–k analysis are located on the north side of the valley. The array beam pattern for this configuration is given in Fig. 9. The first aliasing peak was identified at $k_{\text{aliasing}} = 0.022$ rad m^{-1}; the maximum wavenumber that can be analysed with this configuration is, therefore, $k_{\text{aliasing}}/2 = 0.011$ rad m^{-1} (e.g. Schisselé *et al.* 2004), indicated by the solid circle in Fig. 9. Due to the elongated shape of the array, the resolution is better in east–west than north–south direction.

f–k spectra are calculated with the high-resolution frequency-wavenumber method (Capon 1969; Kind *et al.* 2005) by the *continuous array processing (CAP)* program (Ohrnberger *et al.* 2004; Wathelet 2001). This code is part of a larger software package created in the framework of the SESAME project (available at http://www.geopsy.org).
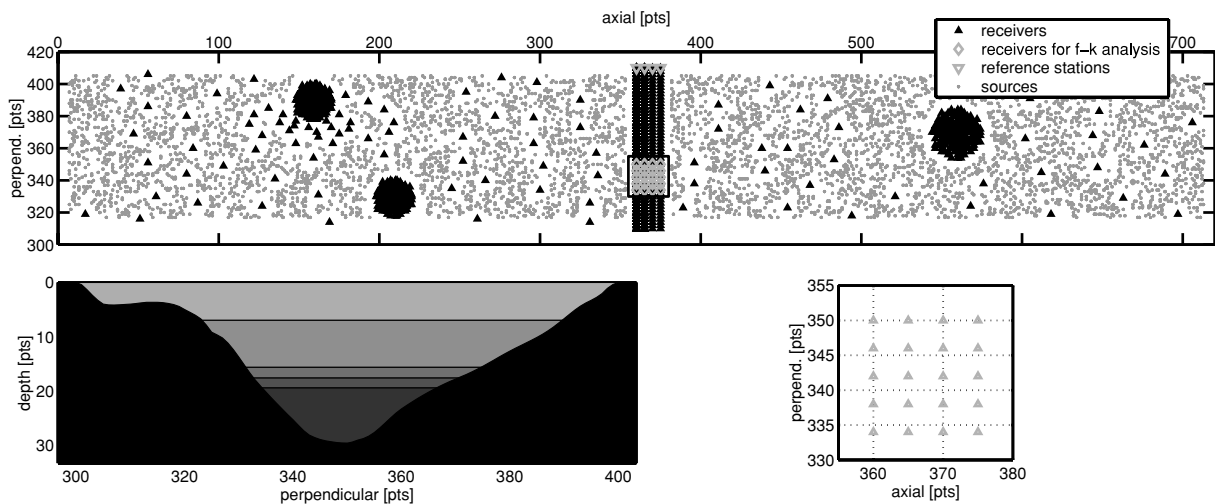
4.5 3-D Numerical simulations

The numerical ambient noise simulation was performed with the program package *NOISE* developed within the SESAME project. (Moczo *et al.* 2002; Moczo & Kristek 2002). This package provides the programs *ransource* and *FDSIM*.

Ransource creates a set of randomly distributed sources and generates a random direction of acting single body force, time function and maximum amplitude for each source. The time function is either a delta-like signal or a pseudo-monochromatic function of random duration and frequency. We placed all sources on the surface of the sediment cover in the valley (Fig. 10).

The wave propagation of this source is simulated with *FDSIM*. This code uses an explicit heterogeneous finite-difference scheme which is fourth-order accurate in space and second-order accurate in time. The computation region is represented by a viscoelastic half-space with 3-D surface heterogeneities and a planar surface (Moczo *et al.* 2001; Kristek *et al.* 2002).

The FD-grid is staggered and consists of a finer grid on top and a coarser grid below. We used 721 × 109 × 40 cells for the fine and 241 × 37 × 11 cells for the coarse grid with a spacing of 30 and 90 m, respectively. The velocity model varies only along two

exactly in phase, the maximum is reached at a lag of zero; if they are in antiphase, the maximum should occur at half the period of the signals.

4.4 f–k analysis

Peaks in the transfer function of an alluvial valley may result from both 1-D resonance and horizontally propagating surface waves as well as from 2-D resonance (Bard & Bouchon 1980). The in- and antiphase pattern expected for the fundamental *SV* mode of 2-D resonance may also be explained with propagating Rayleigh waves generated symmetrically at the valley edges (Gaffet *et al.* 1998; Chávez-García & Stephenson 2003).

To distinguish between horizontally propagating surface waves and standing waves caused by 2-D resonance, we will calculate

Figure 10. *Top:* Source and receiver distribution used for numerical simulation of microtremor. Distances are in grid points, the grid spacing is 30 m. *Bottom left:* Cross-section of velocity model. *Bottom right:* Enlarged section showing the array used for f–k analysis.

dimensions and corresponds to the profile given in Fig. 1 and Table 1. The simulation was performed in the frequency range between 0.25 and 2.35 Hz.

A number of receivers are distributed regularly along the valley surface; another set of receivers is placed to form four parallel lines running perpendicular to the profile axis, with one station on bedrock. The remaining receivers are arranged in three dense arrays on the surface (Fig. 10).

The numerical simulation was running for 6 weeks on an IBM MPP at the Swiss National Supercomputing centre and resulted in about 90 s of synthetic ambient noise.

5 PROPERTIES OF THE SYNTHETIC AMBIENT VIBRATION WAVEFIELD

We will first identify the 2-D resonance frequencies in our synthetic ambient noise.

5.1 Spectral ratios

All sources are located on the sediment surface in our simulation. The reference station method will, therefore, not remove source and path effects. Due to the large impedance contrast between sediment and bedrock, only a small fraction of energy reaches receivers outside the valley, and spectra at these stations are almost flat compared to stations in the valley (Fig. 11). This is quite different from the situation observed in reality (Fig. 17 left). We must keep in mind that spectral ratios applied to our synthetic data will show effects of sources as well as the response of the valley.

Fig. 12 gives spectral ratios of the signals from the receivers located on the line at axial grid position 360 calculated with the reference station at perpendicular grid position 410 (Fig. 10). The spectra are quite heterogeneous, with a lot of peaks at different frequencies. The fundamental mode SV_0 was identified at 0.35 Hz, with two peaks visible on the vertical (top) and one broad peak on the perpendicular component (centre). This is very close to the value of SV_0 reported by Steimen *et al.* (2003) from 2-D simulations. On the axial component (bottom), the fundamental SH_{00} and first higher mode SH_{01} of SH resonance can be identified easily at 0.30 and 0.39 Hz, respectively.
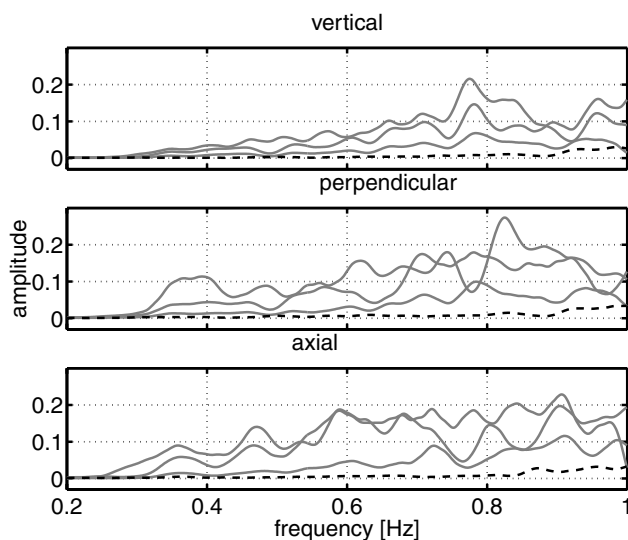
Figure 11. Amplitude spectra calculated from synthetic noise of receivers located on bedrock (black, dashed) and on the sediment (grey, solid) .
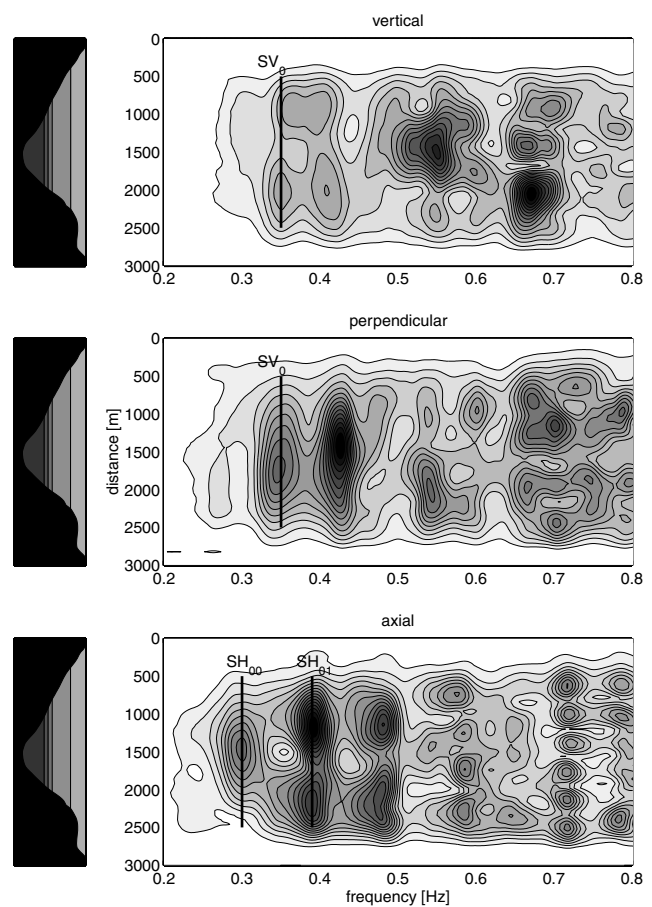
Figure 12. Spectral ratios of points located on profile at axial grid position 360 as a function of distance along the profile and frequency.

Fig. 13 (very right) shows a cross-section of the perpendicular and vertical spectral ratios at 0.35 Hz for all four profiles. The pattern is similar to the SV_0 fundamental mode predicted by theory (Fig. 4), with one central peak on the perpendicular and two peaks on the vertical component (Fig. 4). A certain variability in spectral ratio amplitudes can be observed for the four different profiles. Cross-sections of the axial component at the fundamental and first higher mode are displayed in Fig. 13 (left and centre). At the fundamental mode SH_{00} frequency of 0.30 Hz, all cross-sections exhibit a well-defined single peak, but different amplitudes. The first higher mode SH_{01} (0.39 Hz) is characterized by a central node and two maxima at axial grid positions 360. At this frequency, the four sections are quite different in shape and amplitude.

5.2 Phase behaviour

If the peaks at 0.35 and 0.30 Hz identified from spectral ratios are caused by fundamental 2-D resonance modes, the synthetic ambient vibration wavefield at these frequencies should also exhibit the phase behaviour behaviour predicted by theory as summarized in Fig. 4.

Fig. 14 shows a section of synthetic ambient noise records band-pass filtered at the corresponding SV_0 and SH_{00} fundamental mode frequencies. On the perpendicular component, motion is in phase on all points across the profile. On the vertical component, a phase reversal occurs at the valley centre, and receivers on the one side of the valley are moving in antiphase with receivers on the other side. The axial components are also in phase on all stations across the
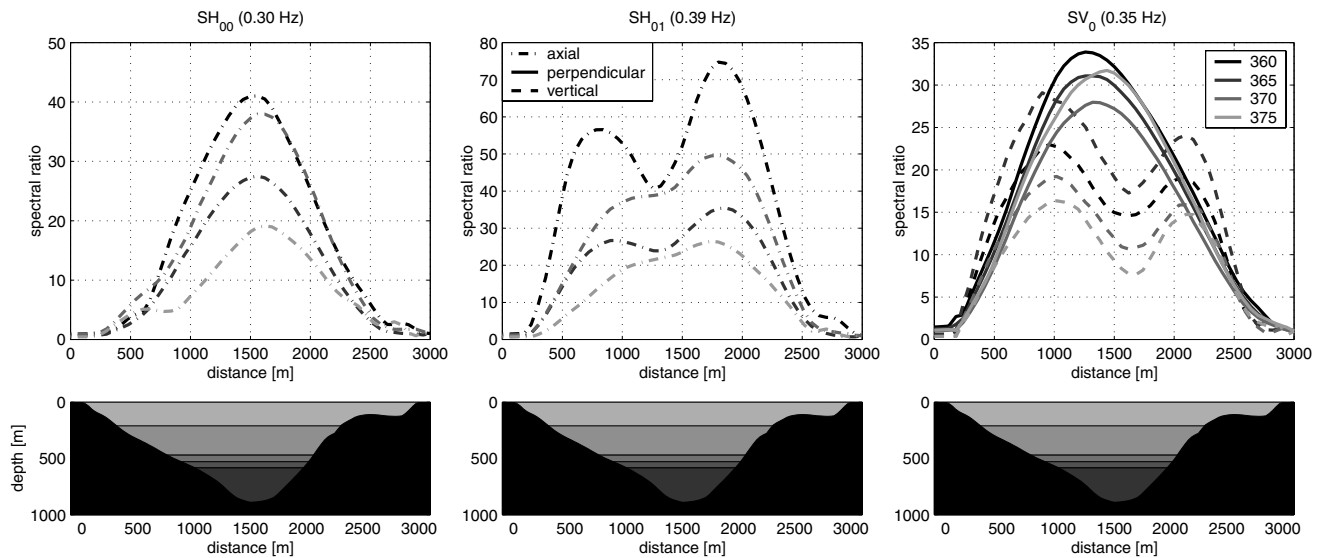
Figure 13. Cross-sections of perpendicular (solid), vertical (dashed), and axial (dash-dotted) spectral ratios at different resonance frequencies for all four profiles.
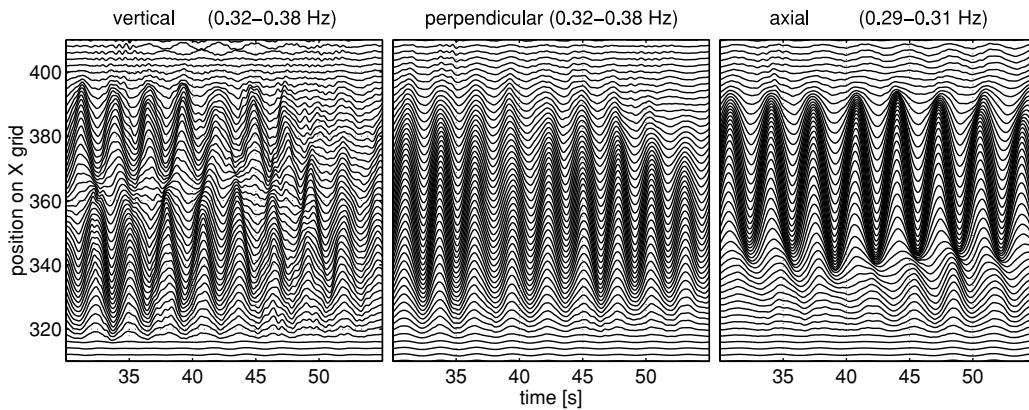

Figure 14. Bandpass filtered synthetic ambient noise records for all points on profile at axial grid position 370. The bandpass was applied at the SV_0 (vertical, perpendicular) and SH_{00} (axial) fundamental mode frequency.

valley. These observations are, therefore, consistent with the behaviour predicted by theory (Fig. 4).

5.3 *f–k* analysis

We calculated *f–k* spectra from synthetic noise, using 20 stations from the four profiles on the lower half of the valley as an array (Fig. 10). The array geometry is, therefore, grid–shaped, with station-intervals in the perpendicular and axial directions of 120 and 150 m respectively; the array aperture is 480 m in the perpendicular and 450 m in axial direction. The array beam pattern for this configuration is given in Fig. 15.

Fig. 16 (top) shows spectra as a function of slowness and azimuth for the vertical and perpendicular component at 0.35 (SV_0) and the axial component at 0.30 Hz (SH_{00}). The peaks at 0.35 and 0.30 Hz are located very close the origin, at slownesses of less than 0.25 s km^{-1}. This means that the disturbance reaches all receivers at nearly the same time, which may be explained with a wave front propagating almost vertically at a slight angle. This is the case for standing waves expected in the case of 2-D resonance.

However, horizontally propagating waves do occur at higher frequencies: at 1.00 Hz (Fig. 16 bottom), multiple peaks appear at

higher slownesses on the vertical axis. This beam pattern develops if Rayleigh waves propagate through the array from different directions. The phase velocity of about 500 ms^{-1} (2 s km^{-1}) corresponds to the 1-D phase velocity at 1 Hz (Fig. 2) calculated from the sediment fill of the velocity model (Table 1).

6 EVIDENCE OF 2-D RESONANCE IN OBSERVED AMBIENT VIBRATIONS

Using the spectral ratio method, we will now determine the frequencies of possible resonance modes in recorded ambient vibrations. Then we will analyse the wavefield properties at the identified frequencies.

6.1 Reference spectra

6.1.1 2002 experiment

Fig. 17 shows average spectra and average spectral ratios calculated from noise recorded during the 2002 experiment. Spectra of reference stations (black) are quite characteristic for sites located inland, with a peak at 0.20 Hz related to oceanic microtremor. Application
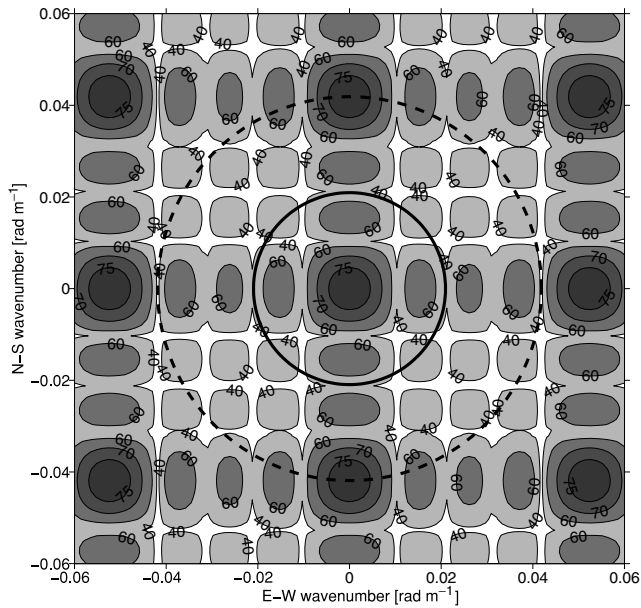
Figure 15. Beam pattern of array configuration for f–k analysis of synthetic microtremors. Contour intervals are indicating the array response in dB. The dashed circle indicates the wavenumber where the first aliasing peaks occur and the solid circle shows the Nyquist wavenumber.

of the spectral ratio method removes this peak from stations located in the valley.

Spectral ratios of the vertical and perpendicular component show a very clear peak at around 0.35 Hz; a secondary peak can be identified at 0.38 Hz. On the axial component, the first peak is located at 0.31 Hz; further peaks can be seen at around 0.43 and 0.50 Hz.
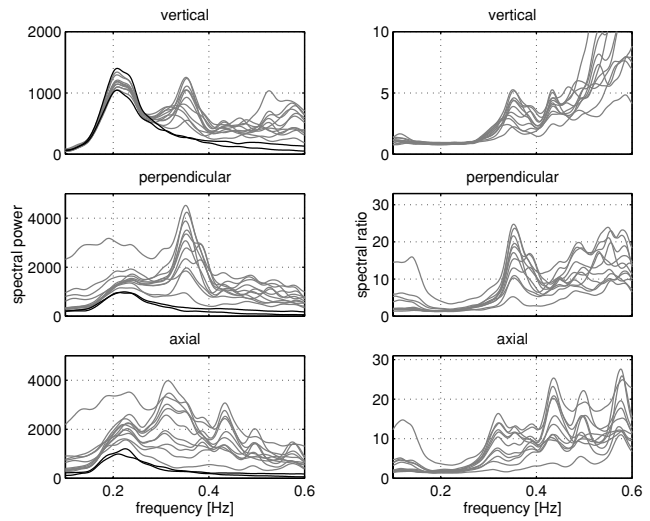
Figure 17. Average power spectra (*left*) and average spectral ratios (from the reference station in the North, *right*) calculated from ambient noise recorded during the 2002 Vétroz experiment. Power spectra of reference receivers located on bedrock are plotted black.

Fig. 18 shows spectral ratios at 0.35 Hz as a function of distance along the profile for the vertical and perpendicular component. The pattern of spectral amplitude for points located on the profile axis (points connected with lines in Fig. 4) is very close to that expected for the SV_0 mode, with a maximum in the valley centre for the perpendicular component and two maxima and one central node for the vertical component.

Similarly, average spectral ratios of the axial component at the resonance frequency of the fundamental SH_{00} mode (Fig. 19 top) compare well with the expected pattern (Fig. 4) for points located on the profile axis.
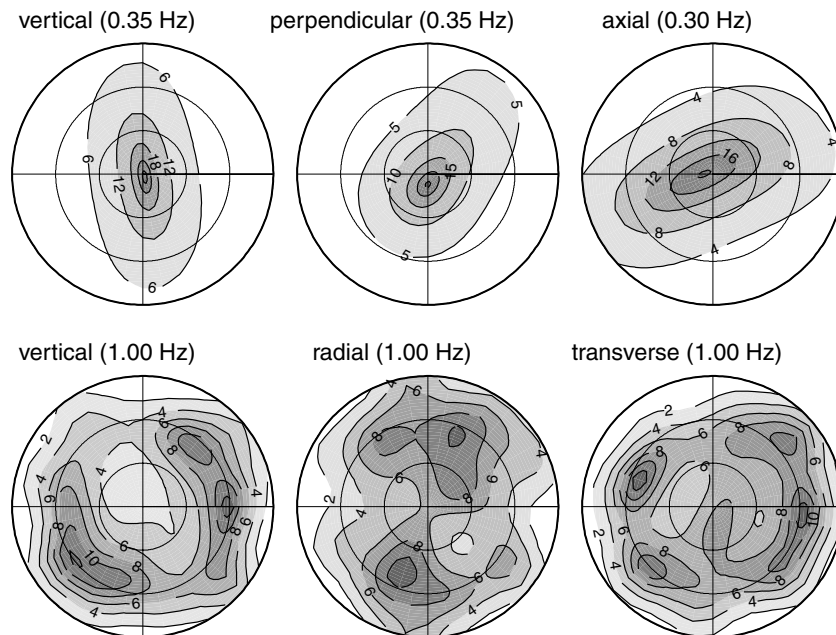
Figure 16. f–k spectra as a function of slowness and azimuth for SV_0 and SH_{00} (top) and at 1.00 Hz, where propagation dominates (bottom). Azimuthal directions are like in Fig. 10, with up/down pointing along the perpendicular and left/right along the axial valley axis. Slowness starts at zero (middle) and reaches 3 s km^{-1} at the outermost ring; concentric grid-lines denote slowness intervals of 1 s km^{-1}. Contour intervals are given in dB. The aliasing slowness is outside the plotted range and not shown.
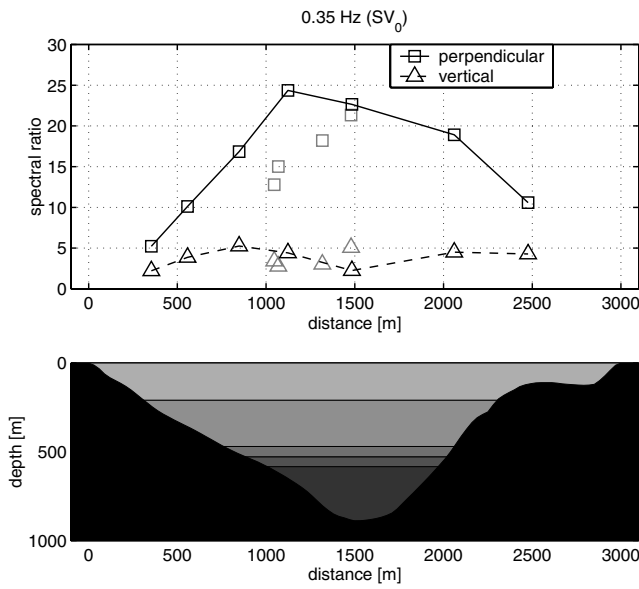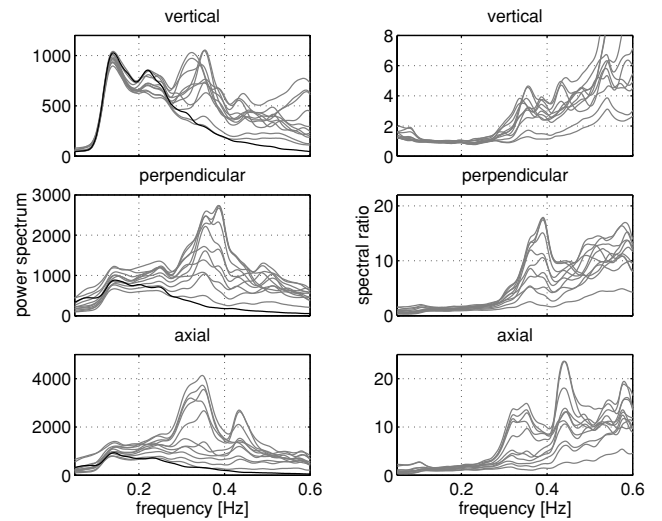
Figure 18. Average site-to-reference spectral ratios for ambient noise recorded in the 2002 experiment for vertical and perpendicular component as a function of distance along the profile (from North to South). Points located on the profile axis (Nr. 02-08 in Fig. 7) are connected with lines and plotted black, points located away from the axis are plotted grey. The reference station is 'Ref N' shown in Fig. 7.
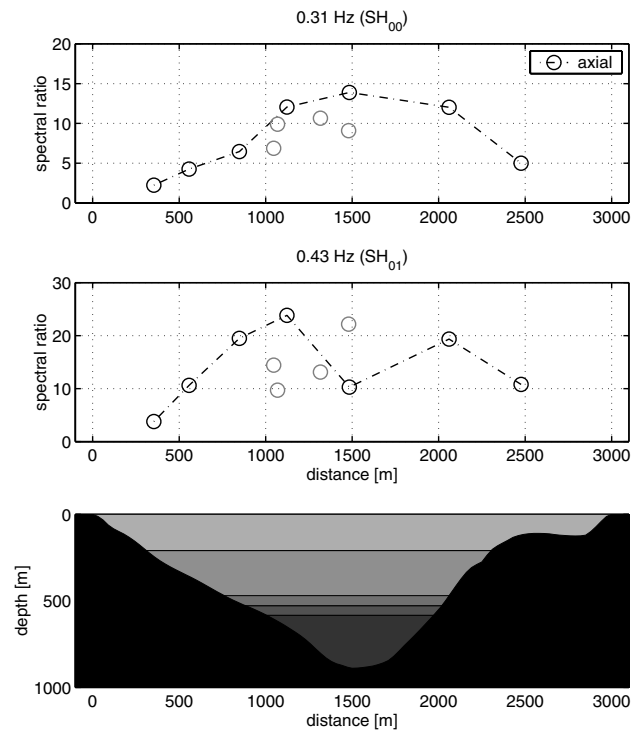
Figure 19. Average spectral ratios of 2002 experiment for axial component as a function of distance along the profile at 0.31 (top) and 0.43 (bottom) Hz. Points located on the profile are connected with lines.

Average spectral ratios at 0.43 Hz (Fig. 19 bottom) for points on the profile are indicating a central node and two peaks, which corresponds to the amplification expected for the first higher mode SH_{01}.

Figure 20. Average power spectra (*left*) and average site-to reference spectral ratios (*right*) calculated from ambient noise recorded during the 2003 Vétroz experiment (first configuration). Power spectra of reference receivers located on bedrock are plotted black. The reference station is 'Ref' shown in Fig. 7.

However, spectral ratios at stations deployed away from the profile (isolated, grey points in Figs 18 and 19) are quite different from stations placed on the profile. This variability along the valley axis was also observed in spectral ratios calculated from the four profiles in the numerical simulation (Fig. 13).
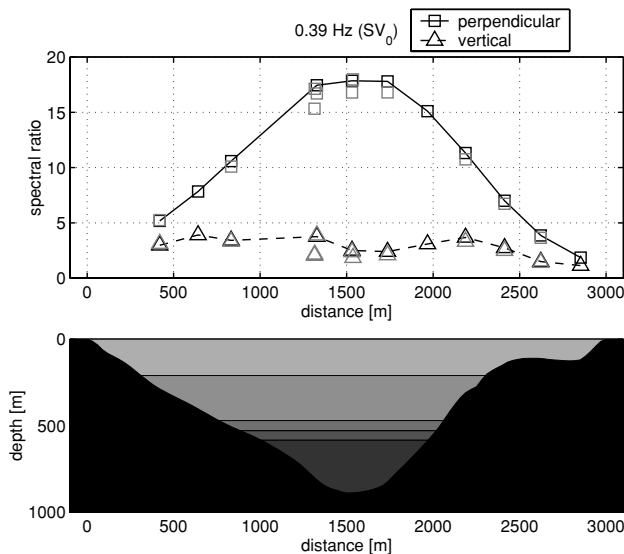
6.1.2 2003 experiment

Fig. 20 shows average power spectra and spectral ratios obtained from the first configuration of the 2003 experiment. The regular, dense station coverage along the profile used for the first configuration of the 2003 experiment (circles and triangles in Fig. 7) allows us to display spectral ratios as a function of distance along the profile in a contour diagram (Fig. 21).

The peaks of the fundamental mode SV_0 resonance are hardly visible in the vertical component, but very obvious for the perpendicular component, where the maximum amplitude is reached at around 0.39 Hz; this is slightly higher than the frequency of 0.35 identified in the 2002 experiment. On the axial component, modes SH_{00} and SH_{01} can easily be identified at 0.35 and 0.43 Hz, respectively; the frequency of the fundamental mode is again quite higher than the value derived from the first experiment. However, the peaks associated with the fundamental modes are quite broad. From Fig. 20, it cannot be excluded that the fundamental mode SV_0 and SH_{00} frequencies are still located at 0.35 and 0.31 Hz respectively for this profile. The four peaks at 0.58 Hz (Fig. 21) might be associated with the fourth higher mode of SH resonance, consistent with the observation in Fig. 17; the third higher mode cannot clearly be identified.

A cross-section of Fig. 21 at 0.38 Hz (Fig. 22) shows an amplitude pattern similar to the one observed at 0.35 Hz in the 2002 experiment, with high amplification and one central peak for the perpendicular and two peaks with low amplifications for the vertical component. Both configurations yield similar amplification patterns. For the second configuration, differences in amplitude between points located on and away from the profile axis can again be observed. (Fig. 22).
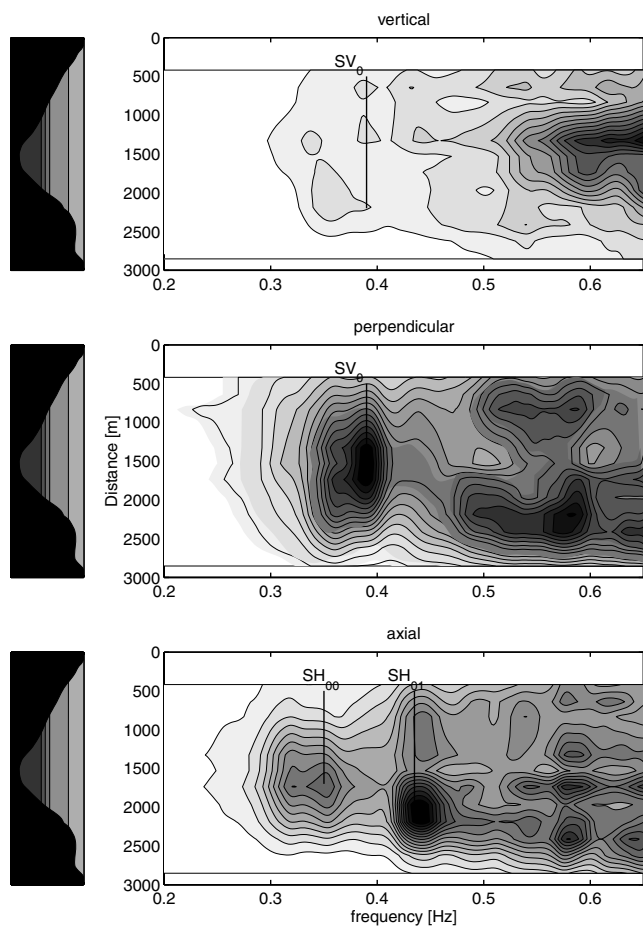
Figure 21. Average spectral ratios as a function of distance along the profile for ambient noise recorded at all stations used in the first configuration of the 2003 experiment.

Figure 22. Average spectral ratios of 2003 experiment (first and second configuration) for vertical and perpendicular component as a function of distance along the profile at frequency 0.39 Hz, interpreted as mode SV_0. Values for the first configuration are connected with lines and plotted black.
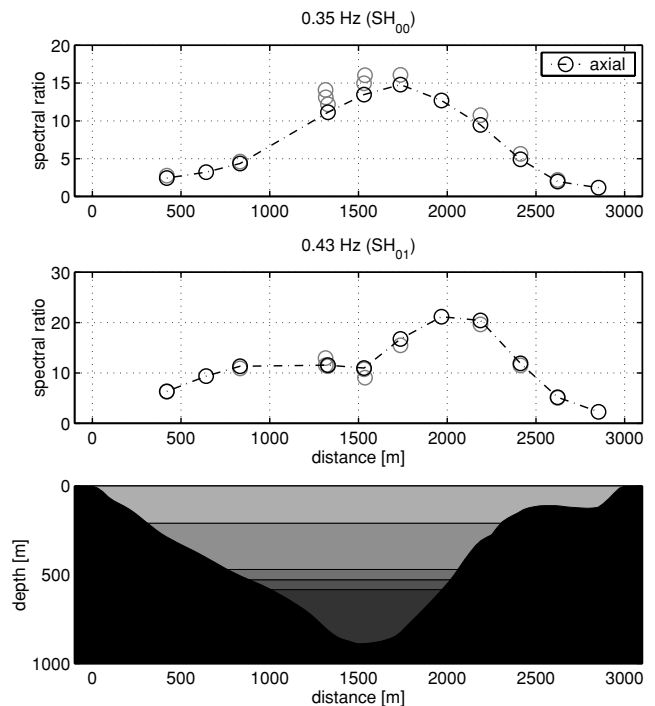
Figure 23. Average spectral ratios of 2003 experiment (first and second configuration) for the axial component as a function of distance along the profile at frequencies 0.35 (top) and 0.43 (bottom) Hz, interpreted as modes SH_{00} and SH_{01} respectively. Values for the first configuration are connected with lines and plotted black.

Cross-sections at the SH_{00} frequency of 0.35 Hz (Fig. 23 top) are reproducing the pattern observed at 0.31 Hz in the 2002 experiment (Fig. 19 top). The second configuration yields higher spectral ratios than the first one. The amplitude pattern at the SH_{01} frequency (Fig. 23 bottom) slightly resembles the pattern observed for the 2002 experiment (Fig. 19 bottom) with two peaks and one node (the low amplitude of the first peak might be explained with the missing station). For both frequencies, the second configuration reveals the variability of spectral ratios along the valley axis.

Table 2 compares resonance frequencies identified in the 2002 and 2003 experiments and in the 3-D numerical simulation with values reported by Steimen *et al.* (2003) and calculated with the method of Paolucci (1999).

6.2 Phase behaviour

In the fundamental mode of SH resonance, the axial motion is in phase on all points across the valley (Fig. 4). If the peak at 0.35 Hz in the spectral ratio is caused by the fundamental SH_{00} mode, this behaviour should also be visible on recorded bandpass filtered traces in this frequency range. Fig. 24 (top) shows axial components filtered between 0.28 and 0.34 Hz for all stations, demonstrating that both stations along the profile and stations outside the profile axis are in phase as expected. The time window from Fig. 24 also displays the increase in amplitude towards the valley centre.

Fig. 25 shows a similar plot for perpendicular and vertical traces bandpass filtered around the SV_0 frequency. While the perpendicular motion is in phase at all points, the phase of the vertical component changes in the valley centre, leading to an antiphase motion at point 7 and 8 on the South side. This observation is consistent with the
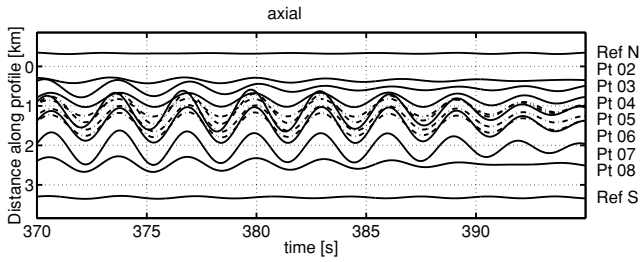
Figure 24. Time window of ambient noise recorded on the axial components during the 2002 experiment bandpass filtered around SH_{00} between 0.28 and 0.34 Hz. Seismograms of points outside the profile are printed with dashed lines.
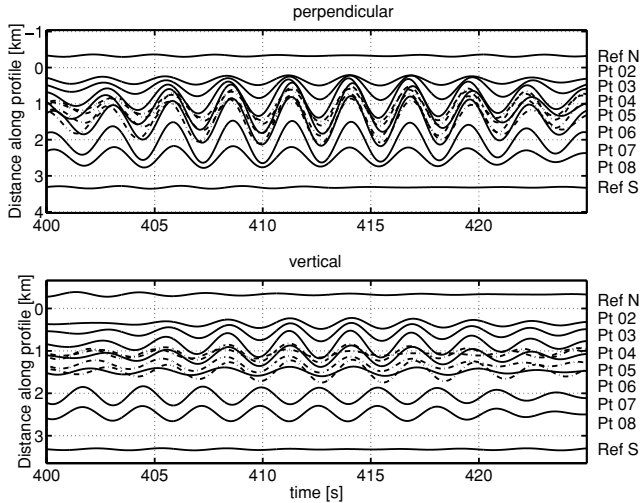

Figure 25. Time window of perpendicular (top) and vertical (bottom) components bandpass filtered around SV_0 between 0.32 and 0.38 Hz. Seismograms of points outside the profile are printed with dashed lines. (2002 experiment)

pattern predicted for SV_0 by theory (Fig. 4) and observed in synthetic ambient vibrations (Fig. 14).

We will now apply the cross-correlation method described above to analyse the dominant phase behaviour of the whole record length. Fig. 26 shows cross-correlation maxima as a function of distance along the profile axis for the perpendicular, vertical (top) and axial (bottom) component. Signals were bandpass filtered around the fundamental mode SV_0 (0.32 to 0.38 Hz) and SH_{00} (0.28 to 0.34 Hz) frequency. On the axial axis (bottom), the maximum of the cross-correlation is reached for very small lags at all points within the valley, including those located away from the profile axis. This shows that the in-phase motion observed in Fig. 24 is the dominant behaviour of ambient noise in this frequency range.

Similarly, cross-correlation maxima on the perpendicular component are obtained for very low lags. On the vertical component, however, the maximum cross-correlation is only around zero for points on the Northern valley side. At point 7 and 8, the maximum is reached for a lag of -1.32 s; this corresponds to half the period of a 0.38 Hz oscillation. This confirms the pattern predicted by theory for SV_0 and observed in Fig. 25, that of in-phase motion on the perpendicular axis and a phase change in the valley centre on the vertical axis.

Application of the above method to ambient noise recorded during the 2003 Vétroz experiment produces very similar results
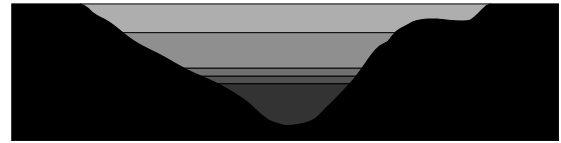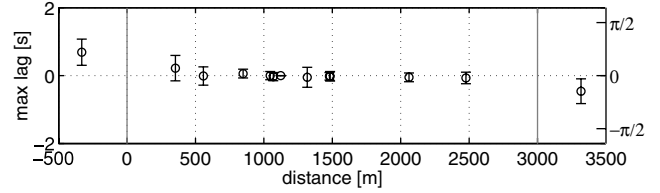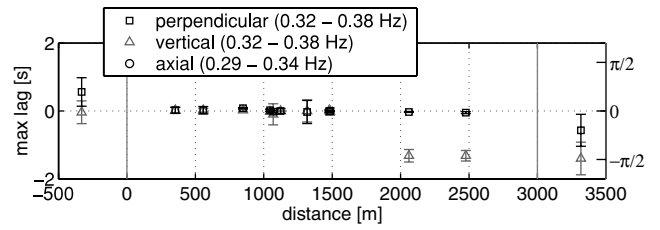

Figure 26. Cross-correlation maxima of perpendicular and vertical (top) and axial (bottom) component as a function of distance along the profile (2002 experiment). Error bars are estimated with the value of the cross-correlation maximum. Signals were bandpass filtered around SV_0 (0.32–0.38 Hz, top) and SH_{00} (0.29–0.34 Hz, bottom). Ticks on the right vertical scale show the phase calculated from the mean value of the frequency band.
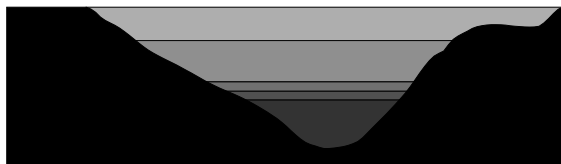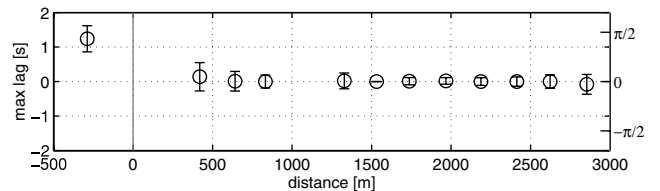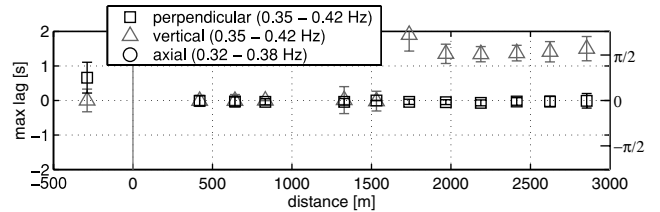

Figure 27. Cross-correlation maxima of perpendicular and vertical (top) and axial (bottom) component as a function of distance along the profile (2003 experiment, first configuration). Error bars are estimated with the value of the cross-correlation maximum. Signals were bandpass filtered around SH_0 (0.35–0.42 Hz, top) and SH_{00} (0.32–0.38 Hz, bottom).

(Figs 27 and 28). For points on the South side, the maximum is reached for lags between 1.28 and 1.50 Hz on the vertical component, which yields a frequency of 0.33 to 0.39 Hz if the signals are in antiphase. The outlier at point 8 (vertical) might be explained with the vicinity to the node; the value of the maximum correlation at this point is very low.
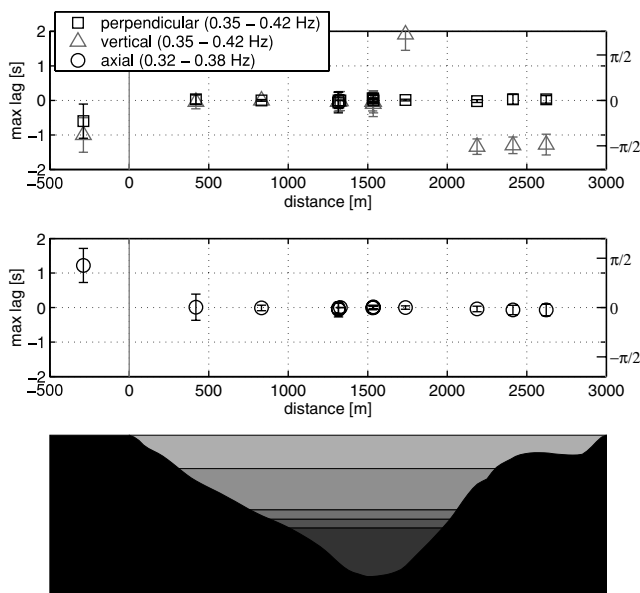
Figure 28. As for Fig. 27, but for the second configuration of the 2003 experiment.
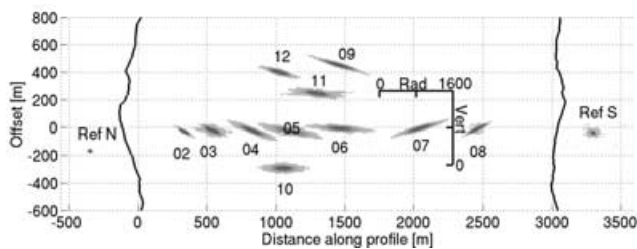
Figure 29. Particle motion plot of perpendicular vs. vertical component obtained from traces bandpass filtered between 0.32 and 0.38 Hz with noise recorded during the 2002 experiment. Areas passed multiple times are shaded dark.

6.3 Particle motion

The motion at the fundamental mode SV resonance is best visualized by a particle motion plot, which is obtained by plotting the perpendicular against the vertical component at each station (Fig. 29). The motion is almost horizontal near the valley centre, where it reaches the highest amplitude. Towards the valley edges, the vertical component is increasing, resulting in an inclined movement. (Fig. 4).

6.4 f–k analysis

Fig. 30 displays results of the f–k analysis obtained from the array of the 2002 experiment. The slowness is displayed in a polar plot as a function of azimuth for the fundamental mode frequencies identified in the 2002 (top row) and 2003 (middle row) experiment at the corresponding components; the lowest row shows f–k spectra for a higher frequency of 0.70 Hz.

The peak in the f–k spectrum is located in the origin of the plot at a slowness of zero at the fundamental mode frequencies of the perpendicular, vertical (SV_0) and axial (SH_{00}) component. This implies that the disturbance reaches all receivers at almost the same time. This corresponds to the expected pattern in the case of 2-D resonance, where motion is in phase on all points at the same side of the valley. These patterns can, therefore, not be created by horizon-

tally propagating surface waves, but by standing waves as expected in the case of 2-D resonance.

At 0.70 Hz, however, peaks appear well outside the origin at around 1.5 s km^{-1} in the NNE and SSW of the slowness-azimuth spectrum (vertical axis). This slowness corresponds to a velocity of around 670 ms^{-1}, which is comparable to the value of around 600 ms^{-1} obtained from 1-D dispersion analysis of the sediment fill in our velocity model (Fig. 2).

7 DISCUSSION

7.1 Properties of 2-D resonance modes

The patterns of spectral amplitude observed in recorded and synthetic data compare well with patterns predicted by theory, supporting the interpretation of these wavefield properties as a consequence of 2-D resonance. While nodes in the amplification pattern are usually not very distinct, both in recorded and synthetic data (e.g. Figs 18, 23 and 13), this may be explained in terms of interference with 1-D-amplification or effects of nearby sources, which prevent the spectral amplitude at the nodes from becoming very small. A discrepancy between theory and observation is the variability of the spectral amplitude with the position at equal distances from the valley border (e.g. Figs 18 and 19). One possible cause may be the statistical effect of the ambient vibration sources, because some variability was also observed in the synthetic ambient noise field (Fig. 13). Alternatively, these observations might be explained by the imperfectly 2-D structure of the valley.

Observed phase characteristics are also in agreement with theory. Since stations located on the profile as well stations laterally shifted away from profiles are moving in phase (Fig. 26 and Fig. 28), these phase characteristics can hardly be caused by laterally propagating surface waves.

7.2 f–k analysis

Results of the f–k analysis show that motion is not always exactly in phase at the resonance frequencies, because slownesses are slightly larger than zero (up to 0.25 s km^{-1}); this is especially true for the fundamental modes in the simulation (Fig. 16). However, the evidence appears to exclude the possibility that these beam patterns are caused by horizontally propagating surface waves.

A surface wave travelling at a phase velocity of 4000 ms^{-1} does not seem realistic compared with the 1-D dispersion analysis obtained from our velocity model (Fig. 2), unless we completely underestimated the shear-wave velocity of the bedrock.

In our numerical simulation, surface waves of this velocity can be ruled out, since the maximum Rayleigh wave velocity cannot exceed the shear-wave velocity of the bedrock (2890 ms^{-1}).

The low slownesses observed in beam patterns at the resonance frequencies can, therefore, only be explained in terms of standing waves evoked by 2-D resonance.

The P-wave fundamental mode (P_0 in Fig. 4) was not identified in recorded or simulated data. This might be interpreted as a consequence of the physical and geometrical properties of the valley, since the P-mode requires a higher shape ratio (i.e. a deeper valley or lower velocities) than the SH- or SV-mode to develop.

7.3 Resonance frequencies

Resonance frequencies obtained from different methods (Table 2) compare well with each other in general. Significant discrepancies
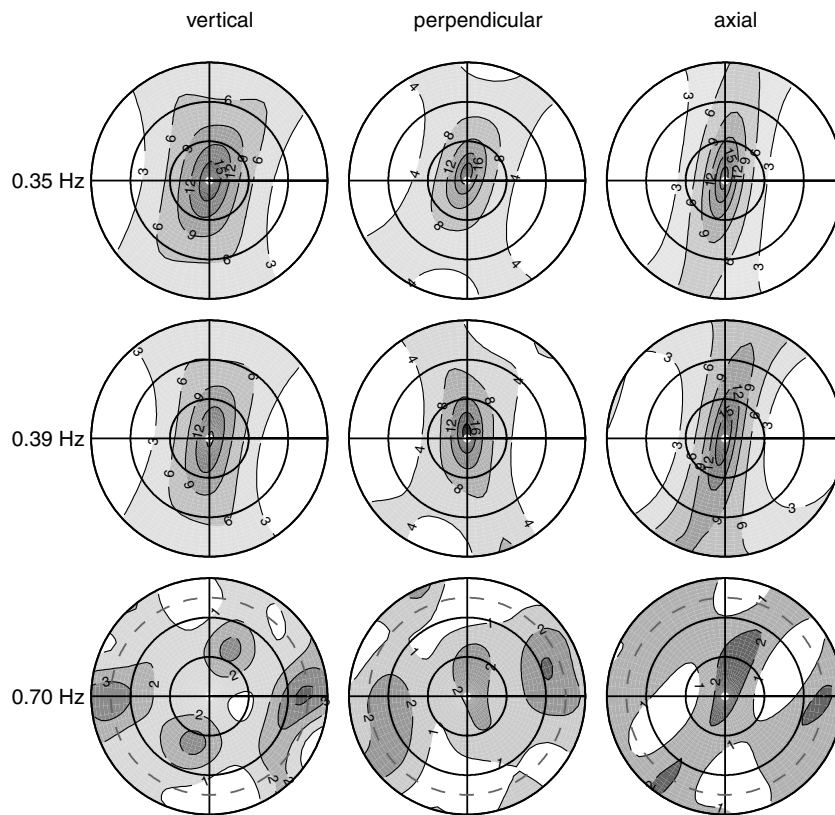
Figure 30. f–k spectra as a function of slowness and azimuth for different frequencies and components. Azimuth is 0 on top (North). Slowness starts at zero (middle) and reaches 3 s km^{-1} at the outermost ring; concentric grid-lines denote slowness intervals of 1 s km^{-1}. Contour intervals are given in dB. The grey dashed line at 0.70 Hz shows the Nyquist slowness.

exist between the fundamental mode frequencies identified from the 2003 experiment and the frequencies derived with other methods and from the 2002 experiment. Given the width of the peaks in spectral-ratio-frequency plots (Figs 17 and 21), these discrepancies are just within the estimated uncertainty. However, the profile of the 2003 experiment is located around 500 m away from the profile used for the 2002 experiment and the seismic reflection profile, which provided most of the geophysical information used for estimation of SV_0 and SH_{00} with numerical simulations and Paolucci's method. It can, therefore, not be excluded that these differences in SV_0 and SH_{00} are caused by lateral variations in the valley geometry.

The frequency of SH_{01} observed in recorded noise is substantially higher than the value obtained from the simulation (Table 2). This difference might be caused by discrepancies between real shear-wave velocities and values used in the geophysical model (Table 1) or by the existence of non-planar layers in the sediment fill.

The uncertainties in the resonance frequencies identified in simulated data are higher than those reported by Steimen *et al.* (2003) (Table 2). This is probably a consequence of exciting the structure with ambient noise originating in the valley instead of laterally incident microtremor energy. Fig. 12 contains a couple of spikes that could not be assigned to a resonance mode (e.g. at 0.40 Hz) and which may be caused by sources located close to the profile. Amplitude spectra at our reference stations (Figs 17 and 20) show that a considerable amount of low-frequency microtremor energy is present outside the valley; this implies that incident waves must contribute significantly to the excitation of 2-D resonance. However, results of our 3-D simulation show that 2-D resonances can

be excited by ambient noise characteristic for urban areas, which is relevant for the applicability of the method.

7.4 Horizontal-to-vertical spectral ratios

The amplification pattern at the fundamental mode SV frequency exhibits a maximum on the perpendicular component and a node on the vertical component around the valley centre (Figs 4, 18 and 22). This suggests that a peak in horizontal-to-vertical spectral ratios will appear around the SV_0 frequency. Fig. 31 (top) shows a contour plot of horizontal-to-vertical spectra calculated from noise recorded during the 2003 experiment. The most conspicuous peaks appear at 0.38 and 0.43 Hz. These frequencies are markedly higher than the expected 1-D resonance frequency of around 0.20 Hz for the sediment fill, and it would be difficult to to assign these peaks to SH_{00}, SV_0 and SH_{01} without our prior knowledge of the noise wavefield.

In order to distinguish between SH and SV resonance, we suggest to calculate the perpendicular/vertical and axial/vertical ratio (Fig. 31 middle and bottom) in the case of deep sediment-filled valleys. SV_0 can easily be identified at 0.38 Hz in the perpendicular-to-vertical contour diagram. SH_{00} is also visible on the axial-to-vertical plot at 0.35 Hz. At the estimated frequency of 0.41 Hz for SH_{01}, only one of the two expected peaks is visible.

These results show that peaks in the horizontal-to-vertical ratio cannot be interpreted in terms of fundamental mode of 1-D resonance in deep sediment-filled valleys; horizontal-to-vertical peaks may be related to fundamental or even higher modes of SV or SH
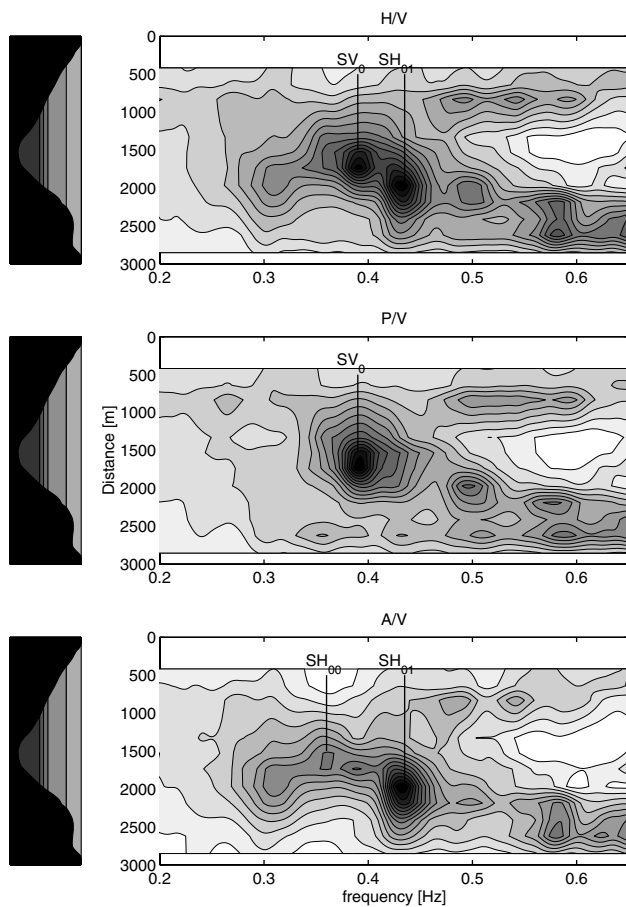
Figure 31. Horizontal-to-vertical spectral ratios as a function of distance along the profile and frequency. Top: horizontal/vertical, centre: perpendicular/vertical, bottom: axial/vertical. (2003 experiment, first configuration.

2-D resonance, depending on the excited mode and on the position in the basin.

The 1-D Rayleigh wave ellipticity in Fig. 2 shows that the fundamental mode horizontal-to-vertical peak would appear at around 0.21 Hz for a horizontally layered structure with the stratigraphy of our model (Table 1). This value is much lower than the peak frequencies obtained from the numerical and experimental methods described in this text, which demonstrates the insufficiency of 1-D analysis to describe the response of this site.

Estimation of either v_s or h from the resonance frequency f_h using the 1-D relation in eq. (2) or 1-D Rayleigh wave ellipticity would not yield useful results in this case.

8 CONCLUSIONS

In summary, our observations imply that the noise wavefield at the Vétroz site is dominated by 2-D resonance at lower frequencies (0.25–0.50 Hz); horizontally propagating surface waves do occur at higher frequencies. We conclude that ambient noise records measured simultaneously on a dense profile may be used to investigate the resonance behaviour of sediment-filled valleys. Simultaneous measurements allow the identification of resonance modes by their phase properties and their horizontal velocity derived from f–k analysis. Horizontal-to-vertical spectral ratios may yield fundamental or higher modes of 2-D resonance, but the identification of the mode is difficult if both horizontal components are used.

REFERENCES

Aki, K. & Larner, K., 1970. Surface motion of a layered medium having an irregular interface due to incident plane SH waves, *J. geophys. Res.,* **75,** 933–954.

Asten, M., 1978. Geological control of the three-component spectra of Rayleigh-wave microseisms, *Bull. seism. Soc. Am.,* **68**(6), 1623–1636.

Asten, M., 2004. Comment on 'Microtremor observations of deep sediment resonance in metropolitan Memphis, Tennessee' by Paul Bodin, Kevin Smith, Steve Horton and Howard Hwang, *Engineering Geology,* **72**(3/4), 343–349.

Asten, M. & Henstridge, J., 1984. Array estimators and the use of microseisms for reconaissance of sedimentary basins, *Geophysics,* **49**(11), 1828–1837.

Bard, P.-Y. & Bouchon, M., 1980. The seismic response of sediment-filled valleys. Part 2. The case of incident P and SV waves, *Bull. seism. Soc. Am.,* **70**(5), 1921–1941.

Bard, P.-Y. & Bouchon, M., 1985. The two-dimensional resonance of sediment-filled valleys, *Bull. seism. Soc. Am.,* **75**(2), 519–541.

Bonnefoy-Claudet, S., Bard, P.-Y. & Cotton, F., 2004. Nature of noise wavefield, SESAME Deliverable D13.8, SESAME EVG1-CT-2000-00026 project (http://sesame-fp5.obs.ujf-grenoble.fr).

Borcherdt, R., 1970. Effects of local geology on ground motion near San Francisco bay., *Bull. seism. Soc. Am.,* **60**, 29–61.

Capon, J., 1969. High-resolution frequency-wavenumber spectrum analysis, *Proceedings of the IEEE,* **57**(8), 1408–1419.

Chávez-García, F.J., Castillo, J. & Stephenson, W.R., 2003. 3D site effects; a thorough analysis of a high-quality dataset, *Bull. seism. Soc. Am.,* **92**(5), 1941–1951.

Chávez-García, J. & Stephenson, W.R., 2003. Reply to 'Comment on '3D site effects: A thorough analysis of a high-quality dataset' by F. J. Chávez-García, J., Castillo, and W. R. Stephenson,' by R. Paolucci and E. Faccioli, *Bull. seism. Soc. Am.,* **93**(5), 2306–2316.

Cornou, C., Bard, P.-Y. & Dietrich, M., 2003. Contribution of dense array analysis to the identification and quantification of basin-edge-induced waves, Part II: application to Grenoble basin (French Alps), *Bull. seism. Soc. Am.,* **93**, 2624–2648.

Fäh, D., Suhadolc, P. & Panza, G.F., 1993. Variability of seismic ground motion in complex media: the case of a sedimentary basin in the Friuli (Italy) area, *J. appl. Geophys.,* **30**, 131–148.

Field, E.H., 1996. Spectral amplification in a sediment-filled valley exhibiting clear basin-edge-induced waves, *Bull. seism. Soc. Am.,* **86**, 991–1005.

Frischknecht, C., 2000. Seismic Soil Amplification in Alpine Valleys. A case study: the Rhône Valley, Valais, Switzerland, *PhD thesis*, Sections des Sciences de la terre, Université de Genève.

Frischknecht, C. & Wagner, J.-J., 2004. Seismic soil effect in an embanked deep Alpine valley; a numerical investigation of two-dimensional resonance, *Bull. seism. Soc. Am.,* **94,** 171–186.

Gaffet, S., Larroque, C., Deschamps, A. & Tressols, F., 1998. Dense array experiment for observation of waveform perturbations, *Soil. Dyn. and Earth. Eng.,* **17,** 475–484.

Gutenberg, B., 1958. Microseisms, *Advan. Geophys.,* **5,** 53–92.

Hermann, R.B., 2002. Computer programs in seismology—an overview of synthetic seismogram computation version 3.30, Department of earth and planetary sciences, St. Louis University.

Kagami, H.D. M.C., Liang, G. & Ohta, Y., 1982. Observation of 1 to 5 second microtremors and their application to earthquake engineering. Part 2. Evaluation of site effect upon seismic wave amplification due to extremely deep soil deposits, *Bull. seism. Soc. Am.,* **72,** 987–998.

Kind, F., Fäh, D. & Giardini, D., 2005. Array measurements of S-wave velocities from ambient vibrations, *Geophys. J. Int.,* **160,** 114–126.

King, J. & Tucker, B., 1984. Observed variations of earthquake motion over a sediment-filled valley, *Bull. seism. Soc. Am.,* **74,** 173–152.

Kristek, J., Moczo, P. & Archuleta, R.J., 2002. Efficient methods to simulate planar free surfaces in the 3D 4th-order staggered-grid finite-difference schemes, *Studia Geophys. Geod.,* **46,** 355–381.

Lermo, J. & Chávez-García, F.J., 1994. Are microtremors useful in site response evaluation?, *Bull. seism. Soc. Am.,* **85**(5), 1350–1364.

Moczo, P. & Kristek, J., 2002. FD code to generage noise synthetics, SESAME deliverable D09.02, SESAME EVG1-CT-2000-00026 project (http://sesame-fp5.obs.ujf-grenoble.fr).

Moczo, P., Kristek, J. & Bystrický, E., 2001. Efficiency and optimization of the 3D finite-difference modeling of seismic ground motion, *J. Comp. Acoustic,* **9**(2), 593–609.

Moczo, P., Kristek, J., Vavrycuk, V., Archuleta, R.J. & Halada, L., 2002. 3D heterogeneous staggered-grid finite-difference modeling of seismic motion with volume harmonic and arithmetic averaging of elastic moduli and densities, *Bull. seism. Soc. Am.,* **92**(8), 3042–3066.

Ohrnberger, M. *et al.*, 2004. User manual for software package CAP—a continuous array processing toolkit for ambient vibration array analysis, SESAME deliverable D18.06, SESAME EVG1-CT-2000-00026 project (http://sesame-fp5.obs.ujf-grenoble.fr).

Paolucci, R., 1999. Shear resonance frequencies of alluvial valleys by Rayleigh's method, *Earthquake Spectra,* **15**(3).

Paolucci, R. & Faccioli, E., 2003. Comment on '3D site effects: a thorough analysis of a high-quality dataset' by F. J. Chávez-García, J., Castillo, and W. R. Stephenson, *Bull. seism. Soc. Am.,* **93**(5), 2301–2305.

Pfiffner, O.A., Heitzmann, S., Mueller, S. & Steck, A., 1997. *Deep Structure of the Swiss Alps—results of NRP 20*, Birkhäuser, Basel.

Schisselé, E., Guilbert, J., Gaffet, S. & Cansi, Y., 2004. Accurate time-frequency-wavenumber analysis to study coda waves, *Geophys. J. Int.,* **158,** 577–591.

Schmid, C., 2000. Eigenfrequenzen von Flusstälern, Semesterarbeit, ETH Zürich.

Seo, K., 1997. Comparison of measured microtremor with damage distribution, in *JICA research and development program on earthquake disaster prevention*.

Steimen, S., Fäh, D., Kind, F., Schmid, C. & Giardini, D., 2003. Identifying 2D resonance in microtremor wave fields, *Bull. seism. Soc. Am.,* **93**(2), 583–599.

Tucker, B. & King, J., 1984. Dependence of sediment-filled valley response on input amplitude and valey properties, *Bull. seism. Soc. Am.,* **74,** 153–166.

Wathelet, M., 2005. Array recordings of ambient vibrations: surface-wave inversion, *PhD thesis*, University of Liège, Belgium.